ICAS-88-4.3.2

AN AERODYNAMIC COMPARISON OF PLANAR AND NON-PLANAR OUTBOARD WING PLANFORMS*

D. A. Naik
Vigyan Research Associates, Inc.
Hampton, Virginia

and

C. Ostowari
Aerospace Engineering Department
Texas A&M University
College Station, Texas

Abstract

The outboard planforms of wings have been found to be of prime importance in studies of induced drag reduction. This conclusion is based on an experimental and theoretical study of the aerodynamic characteristics of planar and nonplanar outboard wing forms. Seven different configurations; baseline rectangular, planar elliptical, planar sheared, sheared with dihedral, sheared with anhedral, rising arc, and drooping arc were investigated for two different spans. Span efficiencies as much as 20% greater than baseline can be realized with nonplanar wing forms, along with, in some cases, no bending moment penalty. The induced drag benefits of non-planar wings are believed to accrue from the movement of vorticity away from the center-of-span line. The resulting downwash distribution can produce induced efficiencies higher than that of a planar elliptical wing. Flow surveys show the accompanying vortex roll-up. Aerodynamic comparisons for the nonlinear lift range are also presented. Parasite drag and lateral stability estimations were not included in the analysis.

Nomenclature

a	lift curve slope
a_o	infinite AR lift curve slope
AR	aspect ratio, b^2/S
b	span
c	reference chord
C_D	drag coefficient, drag/qS
C_l	root bending (or rolling) moment coefficient, moment/qSb; also, sectional lift coefficient where appropriate
C_L	lift coefficient, lift/qS
C_{L_α}	lift slope per degree
C_m	pitching moment coefficient, moment/qSc
C_n	yawing moment coefficient, moment/qSb
C_y	side force coefficient, force/qS
e	span (or induced) efficiency factor
e_1	span effectiveness factor
q	freestream dynamic pressure
RN	Reynolds number w.r.t. c
S	planform area
α	angle of attack

Subscripts

o	zero lift condition
s	stall

*This work was supported by N.A.S.A. Langley. Additional funding was provided by the Aerospace Engineering Department, Texas A&M University.

I. Introduction

There are three broad, inter-related categories into which investigations of induced effects and induced drag reduction fall; the study of the tip vortex, the study of various tip modifications and the study of various planforms. While this paper primarily concerns planform modifications, other considerations are included where necessary. A more comprehensive discussion of related research is given elsewhere[1].

For a subsonic airplane, induced drag comprises roughly one-third of the total drag in cruise[2,3&4] and roughly one-half of the total drag in climb[2]. Since induced drag is inversely proportional to the aspect ratio of the lifting surface[5], the roll-up of the tip vortex is important because this determines the effective span of the wing. The overall drag effects must also be considered because a change in the size of a wing could change the pressure and skin friction drag.

A larger span will only result in better fuel efficiency if there is no corresponding weight penalty incurred by the structural ramifications of increasing the span.[6] Zimmer[7] shows an example in which an increase in span decreases the induced drag by about 11% but increases the structural weight of the wing by 12%. However, in the perspective of the total airplane weight, a 5 to 10 percent increase in the weight of a wing may not be significant as a wing typically is 12 to 20 percent of the total operating empty weight. Good measures of the weight penalty are invariably related to the wing-root bending moment.[6]

It should be duly noted that "some aircraft performance characteristics improve with increasing drag - for example, landing distance and equilibrium rate of descent."[8] Because of these widely divergent requirements, most modern aircraft wings are mechanised for optimum take-off and landing performance. While the present investigation is limited to low subsonic Mach numbers (less than 0.2), some nonplanar effects are more beneficial at transonic Mach numbers.[9]

Ashenberg and Weihs[10] showed that the minimum induced drag of a flat elliptical wing can be obtained "with planforms of both forward and rearward sweep and curvature". van Dam[11] observed that in nature various cruising fish and birds have crescent shaped tails of moderate to high aspect ratio. He used VSAERO[12&13] to "demonstrate that an untwisted planar crescent-moon wing can be more efficient than an unswept elliptical wing."

One reason for considering a nonplanar wing is that a high aerodynamic efficiency is required for a restricted span. Cone[14] used a variation of the lifting line, called the lifting arc, to model the behaviour of nonplanar lifting systems.

For an airplane, the important aerodynamic efficiency parameters for range and endurance are the L/D ratio and the $L^{3/2}/D$ ratio respectively. Cone addressed the following problem: "With the assumption then that an optimum flat wing has been selected for a given aircraft mission, the question arises as to whether other wing forms exist which would possess less drag for the same operating conditions of cruise flight."

Cone proved that "there exists an infinite number of lifting systems which possess less induced drag for a given lift than the optimum flat wing (elliptical planform) of equal span. In fact, many nonplanar wing forms exist which are more efficient, from the induced drag standpoint, than optimum flat wings with greater spans." Of course, the nonplanar wing should not involve structural weight penalties. As modern fabrication techniques and the use of composite materials have resulted in significant advances in wing weight reduction, nonplanar wing forms merit renewed consideration.

Cone calculates that it is possible to get span efficiency factors of greater than one, even up to 1.5, with either nonplanar tip modifications or nonplanar total-span modifications. "Some tip alterations can result in far greater efficiency increases than those produced by radical modification of the entire span. Basically, the greatest increases in span efficiency occur for "modifications which tend to release the major portion of vorticity near the tip and over an appreciable vertical area."

Although "the main aerodynamic characteristics influenced by planform are the induced drag coefficient and the stalling characteristics"[15], there are additional considerations associated with the problem of modifying the outboard planform to increase effective span. The effect on lateral stability could predominate for non-planar outboard wing planforms. To paraphrase the conclusions of van Dam[16]: "To achieve reduction in induced drag," non planar surfaces "produce significant side forces" that "can also seriously affect airplane lateral-directional aerodynamic characteristics."

The work described in this paper deals with planar and nonplanar sheared (swept and tapered) outboard wing forms (similar to those studied by van Dam[17]), and also with circular arc nonplanar outboard forms similar to those studied by Cone. A compromise elliptical outboard planform is also included for comparison. The relatively elementary forms used in this work are merely intended to illustrate trends. They are not intended to represent practical designs.

II. Model description and procedure

The model wing forms are sketched in Fig. 1. Pertinent dimensions and aspect ratios are given in Table 1. The aspect ratios have been defined with respect to the projected area[14].

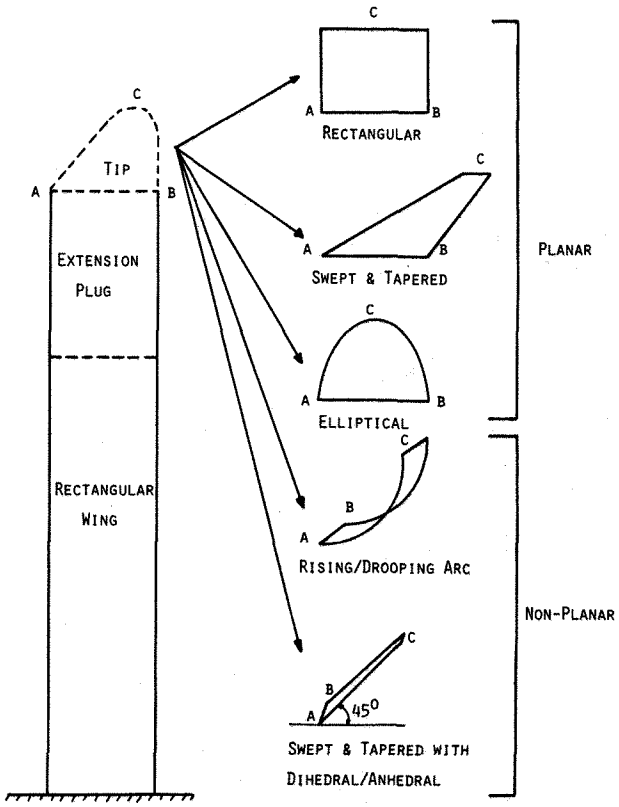

Fig. 1 Model configurations.

In order to properly isolate the effects of the planform modifications, the baseline model was an untwisted, unswept and untapered, rectangular planform with no dihedral. The chord was 1 ft (0.3048 m). The model was of the reflection plane type with the base mount in the tunnel floor. The tip edge was flat. The outboard 0.75 ft (0.2286 m) of the model could be removed and replaced with the planforms described below. A 15% thick symmetrical airfoil section was used. This section, designated[18] WSU 0015, was designed using the Eppler code[19].

Instead of keeping the aspect ratios constant at 8 and 11, it was more convenient to keep the overall model spans constant[20]. The sheared outboard planform had a projected length of 0.75 ft (0.2286 m) root chord of 1 ft (0.3048 m), a tip chord of 0.25 ft (0.0762 m), and a sweepback of 60^{o}. A removeable fillet could be inserted to provide this planform with a 45^{o} dihedral or anhedral while keeping the overall model span constant. Another outboard planform used in this study was a constant-chord circular arc of radius 0.75 ft (0.2286 m). Depending on the orientation of the wind vector, this could be viewed as either a rising arc outboard planform or a drooping arc outboard planform. The elliptical outboard planform had semi minor and major axes of length 0.5 ft (0.3048 m) and 0.75 ft (0.4572 m) respectively.

The experiments were conducted at the Texas A&M University 7 ft x 10 ft (2.13 m x 3.05 m) low speed wind tunnel. The tunnel has a turbulence factor of 1.1. Relevant measurement resolutions are given in Table 2.

Table 1 - Model aspect ratios

Semi-span	1.68 m	1.22 m
Planar[a]		
Baseline	11.000	8.000
Elliptical	11.332	8.335
Sheared[b,c]	11.593	8.605
Non-planar[a]		
Sheared+Dihedral[b,c,d]	11.413	8.419
Sheared+Anhedral[b,c,d]	11.413	8.419
Rising Arc	11.000	8.000
Drooping Arc	11.000	8.000

[a]Outboard planform projected length = 0.2286 m
[b]Sweep = 60°
[c]Taper ratio = 0.25
[d]Dihedral/Anhedral = 45°

Table 2 - Measurement resolution

Quantity	Resolution[a]
C_D	± 0.00015
C_L	± 0.002
C_y	± 0.00075
C_l	± 0.0015
C_m	± 0.0005
C_n	± 0.0005

[a]These are the upper limits. Expected uncertainties will be lower.

A chord RN of 1.3 million was used for the tests. The dynamic pressure needed to achieve this RN is 49 psf (1.13×10^4 Pascals). The freestream wind speed is about 132 ft/sec (40 m/s). The corresponding Mach number is roughly 0.18. The angle of attack range studied was -4° to 20° in increments of, 2° in the linear lift region and 1° in the nonlinear range. Boundary layer trip strips were used to fix the transition location.

The forces and moments were resolved with respect to the quarter chord location on the root section. The measured data was corrected following the standard procedure given in Rae and Pope[21]. In addition, the drag data was corrected for the drag of the trip strips.

The panel method program, VSAERO[13], was used for the analysis of planar and nonplanar outboard planforms. VSAERO allows detailed panelling near the tip region and offers the capability of analysis for a prescribed separation pattern.

The location of the tip vortex, as indicated by the cross-flow velocities, was obtained from 3-dimensional hot film constant temperature anemometer surveys of the flowfield. A planar survey grid perpendicular to the freestream velocity was studied at the 0.2 c downstream location. Because of the probe volume, the grid mesh could not be finer than 0.25 in (6.35 mm). A non-nulling seven-hole probe was then used to obtain more accurate information of the vortex velocities and pressures. The fluorescent oil flow technique was employed for the surface flow visualization studies.

III. Results

To keep matters in perspective, one would like to reiterate that high lift comparisons between configurations are somewhat inappropriate from a practical standpoint as most airplane wings are "mechanized" (with flaps, slats, spoilers, etc.) for better performance in this regime. Nevertheless, the high-lift comparison is necessary for the completeness of a fundamental study of this nature.

The aerodynamic force and moment comparisons between the various planforms are summarized in Tables 3, 4, and 5.

The span effectiveness factor, e_1, was calculated from:[1&22]

$$a = a_o / [1 + a_o/\pi e_1 AR] \quad (1)$$

The span efficiency factors, e_{expt} and e, were calculated by using the experimental and theoretical data respectively in:[1&22]

$$C_D = C_{Do} + C_L^2 / \pi AR e_{expt} \quad (2)$$

Planar wing forms

While the three planar planforms are quite different from a geometrical standpoint, their gross aerodynamic characteristics are closely allied, Table 3. This is despite the noticeably different surface flow patterns (shown for angles of attack of 12 and 18 degrees in a later section). Of the three planforms, the swept and tapered has the best overall performance, but this is only marginally so.

Rising and drooping wing forms

Representative plots, comparing the smaller span baseline, rising and drooping arc configurations are given in Fig. 2. In the interests of more clarity and less clutter, only selected data points have connecting lines passing through them.

For non-planar planforms, efficiency factors greater than one have been predicted by Cone[14]. While the rising arc, drooping arc and baseline wing forms have identical projected area, span and aspect ratio, Table 4 indicates that the rising and drooping arcs have higher span efficiency factors than the baseline. For the lower span, the e_{expt} is greater than one.

Table 3 - Force and moment summary for the planar configurations

Parameter	Baseline	Elliptical	Swept
1.22 m (4.0 ft) semi-span models			
$C_{L\alpha}$	0.082	0.082	0.084
α_s	15.5	15.5	15.5
C_{Lmax}	1.070	1.104	1.098
C_{Do}	0.0133	0.0128	0.0127
e_1	0.69	0.66	0.70
e_{expt}	0.81	0.82	0.79
e	0.95	0.96	0.99
$\lvert\delta C_l / \delta C_L\rvert$	0.6061	0.6018	0.6000
1.68 m (5.5 ft) semi-span models			
$C_{L\alpha}$	0.088	0.088	0.090
α_s	13.8	13.8	13.8
C_{Lmax}	1.118	1.118	1.129
C_{Do}	0.0129	0.0139	0.0125
e_1	0.67	0.65	0.71
e_{expt}	0.78	0.85	0.78
e	0.92	0.94	0.98
$\lvert\delta C_l / \delta C_L\rvert$	0.5386	0.5344	0.5288

Table 4 - Force and moment summary for the non-planar arcs

Parameter	Baseline	Rising	Drooping
1.22 m (4.0 ft) semi-span models			
$C_{L\alpha}$	0.082	0.087	0.084
α_s	15.5	13.5	15.5
C_{Lmax}	1.070	1.151	1.071
C_{Do}	0.0133	0.0149	0.0149
e_1	0.69	0.92	0.75
e_{expt}	0.81	0.82	1.03
e	0.95	1.10	1.09
$\lvert\delta C_l / \delta C_L\rvert$	0.6061	0.6097	0.4815
1.68 m (5.5 ft) semi-span models			
$C_{L\alpha}$	0.088	0.091	0.090
α_s	13.8	12.8	13.8
C_{Lmax}	1.118	1.143	1.103
C_{Do}	0.0129	0.0141	0.0141
e_1	0.67	0.79	0.74
e_{expt}	0.78	0.85	0.78
e	0.92	1.10	1.02
$\lvert\delta C_l / \delta C_L\rvert$	0.5386	0.5457	0.4805

The apparent anomaly, of an efficiency greater than one, is probably related to the definition of geometric aspect ratio being somewhat misleading for non-planar wings, i.e. aspect ratio is always given w.r.t. the projected area. Perhaps, the effective aspect ratio (e x AR) proposed by Cone[14] is a more reasonable indicator of the comparative effectiveness of a particular planform. A higher effective aspect ratio would imply better induced performance.

The nonplanar arc wings both have higher effective aspect ratio than the baseline. For the smaller span these effective aspect ratios are nearly identical (approximately 1.10 x 8.0 = 8.8). However, this higher effective aspect ratio could be physically misleading. The vortex for the rising arc rolls-up off the tip towards the inboard wing resulting in a physically shorter effective span. The vortex for the drooping arc rolls-up away from the wing resulting in a physically wider effective span. For both wings, the calculated effective aspect ratio is greater than the geometric aspect ratio. This means that a physically wider effective span is not the only means to improving efficiency. Rather, a strategic placement of the tip vortex and the resulting downwash distribution are the keys to improving span efficiency.

The nonplanar rising arc has a higher maximum lift coefficient and a sharp, but not severe, stall break, Fig. 2 (a). With the rising arc a considerable drag advantage is gained in high-lift conditions particularly just before stall, Fig. 2 (b). The nonplanar drooping arc is seen to have comparable drag to the baseline in the high-lift regime.

Spanwise circulation distributions for the smaller span models, calculated using VSAERO are shown in Fig. 2 (c). These distributions correspond to an angle of attack of 8^o. For each wing, the "outboard" portion of the planform starts just beyond the 0.80 spanwise station

The distributions serve a dual purpose, i.e. also as spanwise load distributions, because all three configurations are of constant chord. The drooping curve is seen to have marginally higher loading than the baseline. This results in a marginally greater lift. The rising curve has noticeably higher loading throughout.

Some physical insight is needed to account for the difference in circulation between the rising arc and the drooping arc. One possibility is that the tip vortex that rolls-off the end of the rising arc is inboard and above the wing upper surface, whereas the vortex off the drooping tip is outboard and physically below the wing lower surface. These possibilities are examined in the section on the flow surveys.

In any event, even if one discounts the theoretical efficiencies, circulation distributions and induced drags, the experimental force data alone shows that the drooping arc nonplanar wing has many aerodynamic advantages when compared to the baseline. The drawback is the larger zero-lift drag because of the large wetted area. However, it has lower total drag for a large portion of the linear lift range, Fig 2 (b).

The pitching moment curves for the rising and drooping arcs are relatively flat in the linear lift range, Fig. 2 (d).

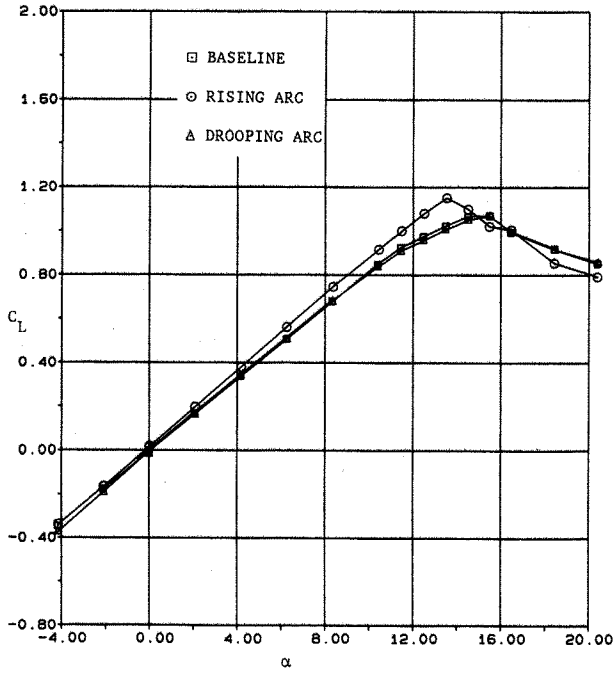

(a) Lift.

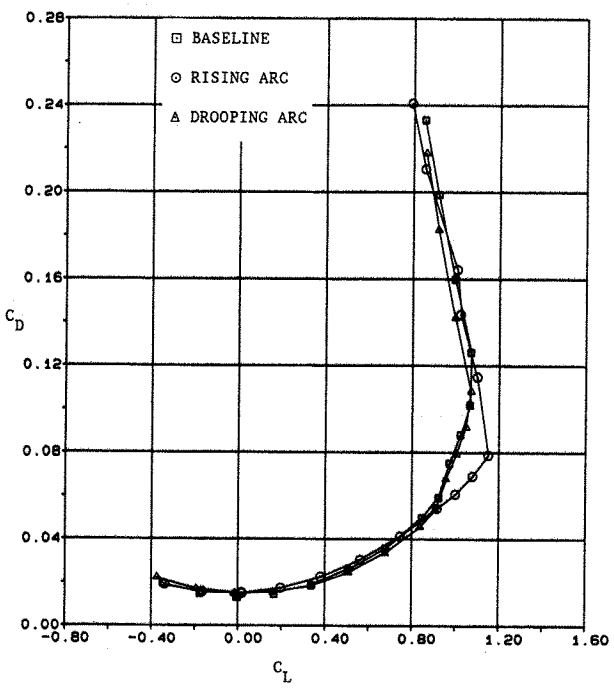

(b) Drag.

Fig. 2 Continued.

Fig. 2 Force and moment data for the smaller span rising and drooping arc planforms.

The primary contributor to the root bending moment (or semi-span rolling moment, Fig. 2 (e)) is the lift force. In addition, a side force generated by the nonplanar portion of the planform increases gradually with angle of attack and as a consequence contributes to the root bending moment through a small moment arm. With the onset of flow separation, the spanwise location of the center of lift changes erratically with changing angle of attack. Hence, the relationship between bending moment and lift is no longer linear.

The (semi-span) yawing moment, Fig. 2 (f), follows parabolic trends in the linear lift range because of its direct dependence on drag. The lower total drag of the drooping arc configuration results in this configuration having the lowest (absolute) yawing moment at any given lift coefficient in the linear lift range.

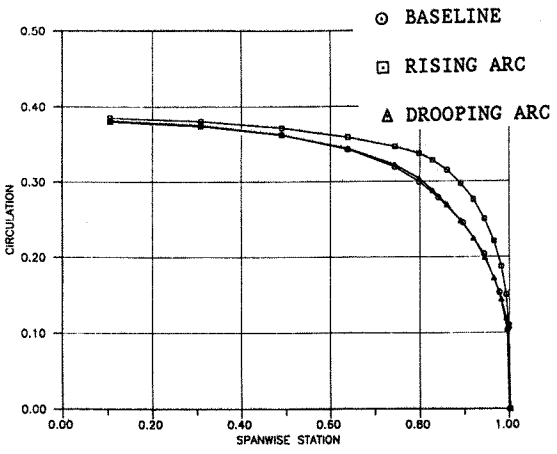

(c) Circulation distributions at $\alpha = 8^{o}$.

Fig. 2 Continued.

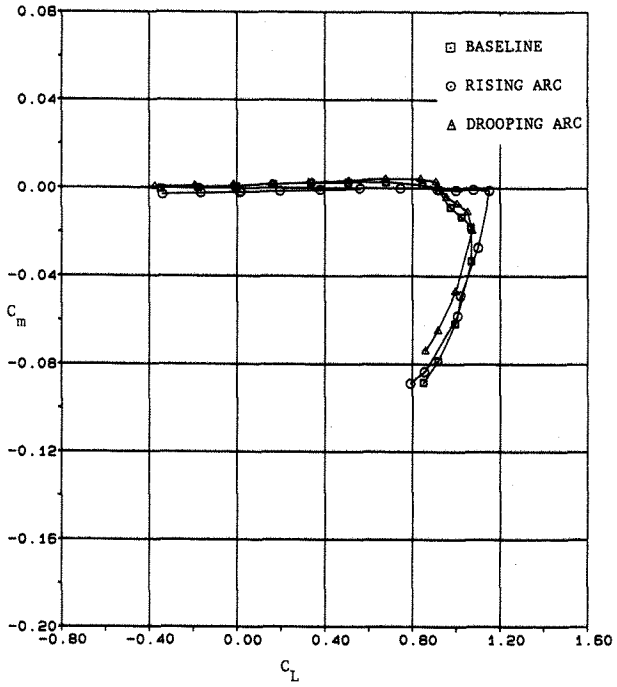

(d) Pitching moment.

Fig. 2 Continued.

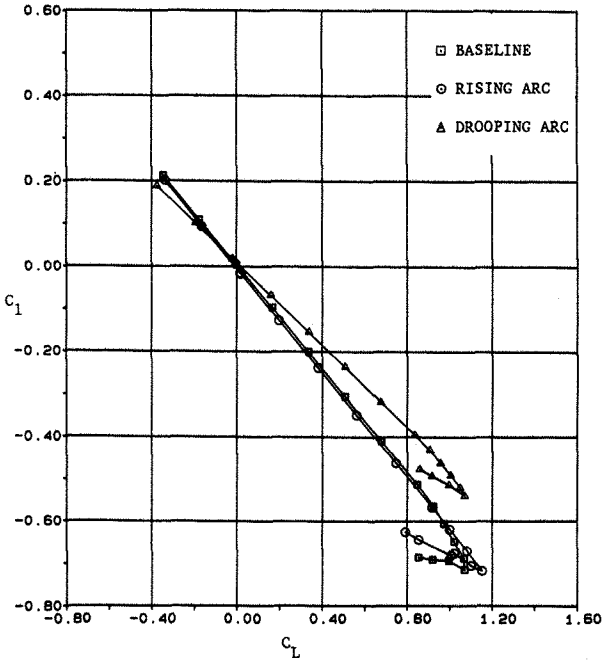

(e) Bending (or semi-span rolling) moment.

Fig. 2 Continued.

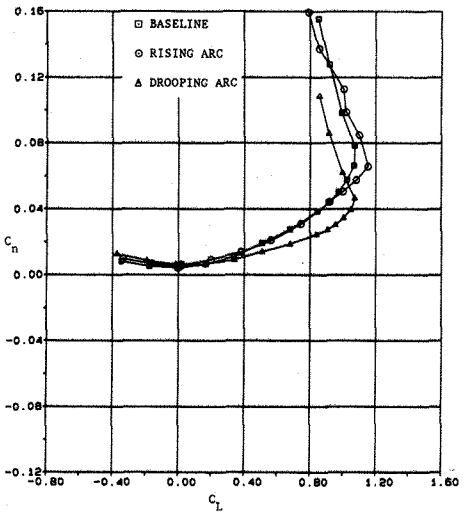

(f) Semi-span yawing moment.

Fig. 2 Concluded.

Sheared with dihedral/anhedral

The nonplanar sheared forms at 45° anhedral or dihedral do not seem to offer any aerodynamic advantages, other than marginally lower bending moment, over the planar sheared, Table 5. VSAERO was used to investigate various nonplanar sheared outboard planforms that were identical in all respects except for the amount of dihedral/anhedral. This work[1] showed that for greater than 45° dihedral/anhedral, both induced drag and root bending moment benefits can be achieved.

Table 5 - Force and moment summary for the sheared models

Parameter	Baseline	Swept	Dihedral	Anhedral
1.22 m (4.0 ft) semi-span models				
C_{L_α}	0.082	0.084	0.081	0.079
α_s	15.5	15.5	14.5	15.4
C_{Lmax}	1.070	1.098	1.118	1.025
C_{Do}	0.0133	0.0127	0.0128	0.0128
e_1	0.69	0.70	0.63	0.57
e_{expt}	0.81	0.79	0.71	0.83
e	0.95	0.99	0.98	0.94
$\lvert\delta C_l / \delta C_L\rvert$	0.6061	0.6000	0.5881	0.4454
1.68 m (5.5 ft) semi-span models				
C_{L_α}	0.088	0.090	0.088	0.085
α_s	13.8	13.8	12.8	14.8
C_{Lmax}	1.118	1.129	1.086	1.107
C_{Do}	0.0129	0.0125	0.0126	0.0126
e_1	0.67	0.71	0.65	0.56
e_{expt}	0.78	0.78	0.68	0.80
e	0.92	0.98	0.98	0.94
$\lvert\delta C_l / \delta C_L\rvert$	0.5386	0.5288	0.5226	0.4526

Flow surveys

Static and total pressure coefficients were obtained by non-dimensionalizing, the local pressure differences from the freestream conditions, w.r.t. the freestream dynamic pressure. For nominally unseparated conditions, i.e. the linear lift range, the vortex is not expected[23] to shift appreciably. This finding was also confirmed here for surveys conducted at 8^o, 10^o and 12^o angles of attack. Thus, it is not improper to compare the vortex locations of different configurations at the same angle of attack.

The vortex locations for the smaller span models are given in Table 6. The locations are accurate to 0.125 in (3 mm). For convenience, the vortex locations, given in Table 6, are sketched in Fig. 3.

Rough quantitative estimates of the size of the tip vortices were made by measuring the extent (average "diameters" as the contours are not circular) for a chosen static pressure. For convenience, the -0.68 static pressure contour was picked. Table 6 also lists these average diameters. These are a means to compare the relative vortex strengths. A more tightly wrapped vortex (smaller diameter) has higher strength.

For all three planar models, the tip vortex is within an inch (2.54 cm) inboard of the tip edge (A, B, C in Fig. 3). However, the vortex (C) for the swept and tapered planform is closer to the wing upper surface. The swept and tapered model and the outboard elliptical model have more tightly wrapped vortices than the baseline model, Table 6. These differences apparently have minimal effect on the overall aerodynamic characteristics (given in an earlier section) of the planar configurations.

Table 6 - Vortex locations and approximate sizes

No.	Configuration	Location[a]	Size[b]
A	Baseline	(0.10 c, 0.995 b/2)	> 0.3 c
B	Elliptical	(0.13 c, 0.984 b/2)	0.3 c
C	Sheared	(0.00 c 0.990 b/2)	0.3 c
D	Rising	(0.79 c 0.984 b/2)	0.3 c
E	Drooping	(0.67 c, 1.010 b/2)	0.2 c
F	Dihedral	(0.63 c, 0.974 b/2)	0.3 c
G	Anhedral	(0.50 c, 0.948 b/2)	0.2 c

[a]These locations are sketched in Fig. 3.
Abcissae are w.r.t. the inboard model plane.
Ordinates are w.r.t. the tunnel floor.
All coordinates are absolute values.
[b]The "size" is the average diameter of the -0.68 static pressure contour.

The vortex for the rising arc (D in Fig. 3) is located roughly three quarters of an inch (2 cm) inboard of the wing tip on the wing upper surface. This spanwise location is comparable to the location for the baseline, elliptical, and swept planforms studied previously. However, the vortex is 0.8 c above the inboard wing plane. For the rising arc the -0.68 static pressure contour is of similar extent, Table 6, to those for the elliptical and swept planar wing forms.

For the drooping arc, the vortex (E in Fig. 3) is roughly half an inch outboard of the wing tip and is 0.67 c below the wing upper surface. The average extent of the -0.68 static pressure contour level is 2.1 inches (5.4 cm). This indicates a more tightly wrapped vortex than those of the other wing forms, Table 6.

The static pressure coefficient is expected to be zero at locations corresponding to the freestream conditions. It decreases as one progress towards the vortex core. Inside the core, this coefficient is expected[24] to reach a plateau at some negative value because of viscous effects. This trend is seen in the contours for the dihedral, Fig. 4 (a), and anhedral, Fig. 4 (b). The grids superimposed on the contours are of size 0.0208 b/2, i.e. 1 inch or 2.54 mm.

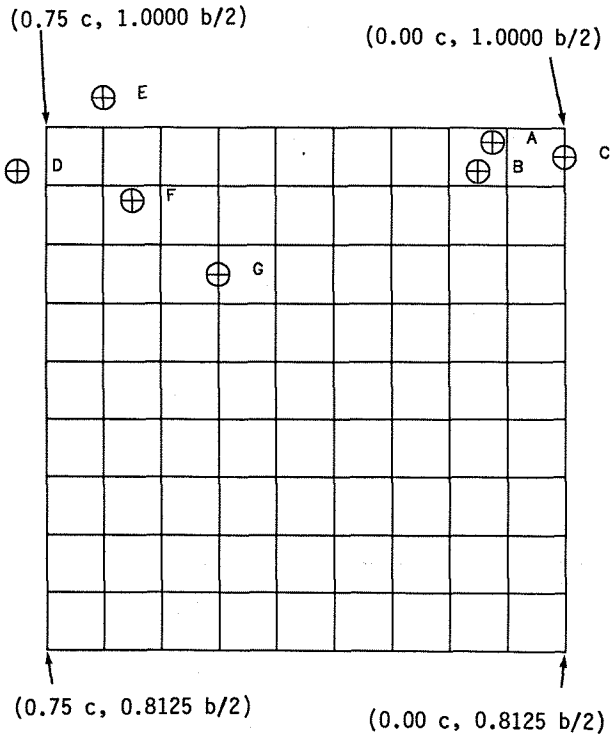

Fig. 3 Vortex locations for the smaller span configurations at $\alpha = 8^o$.

The dihedral model has a vortex (F in Fig. 3) that is more outboard than that of the anhedral model (G in Fig. 3) at the same angle of attack. The dihedral has a larger effective span and a higher efficiency.

These contours are not circular. This was also true of the contours for the other planforms. The skewness probably arises from the presence of secondary vortices. The contours are more like Cassini ovals[25].

Total pressure is expected to be constant in the outer inviscid portion of the vortex. In the core, the action of viscous forces causes a decrease in fluid mechanical energy that is reflected in the decrease in total pressure. The total pressure distribution for the anhedral wing at 8^{o} angle of attack is shown both in the form of contours, Fig. 5 (a), and in the form of a three-dimensional view, Fig. 5 (b).

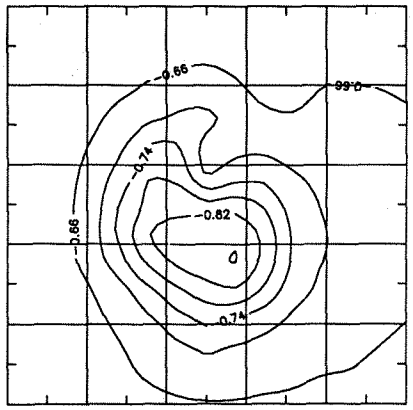

(a) Dihedral.

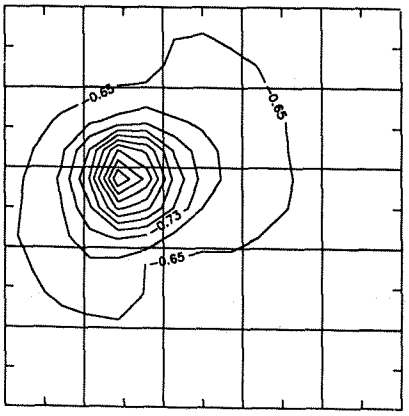

(b) Anhedral.

Fig. 4 Static pressure contours for the smaller span dihedral and anhedral models at $\alpha = 8^{o}$. A one inch (2.54 cm) grid is superimposed on the plot.

The outermost contour corresponds to a total pressure coefficient of -0.04. The inner contours have gradually increasing (in a negative sense) total pressure coefficients. This, again, is in agreement with expectations[24].

The three dimensional view clearly shows the vortex core. There is a region of slightly positive total pressure just outside the vortex core. This apparent anomaly has been observed by other users of a seven-hole probe. The positive total pressure coefficient "may be the result of a transfer mechanism that is not yet understood."[24]

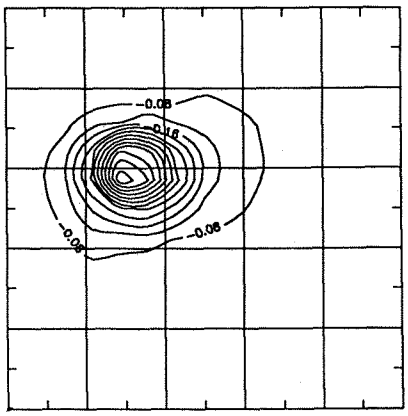

(a) Pressure contours.

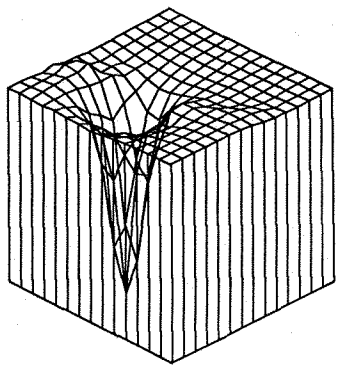

(b) Three-dimensional view of the pressure distribution.

Fig. 5 Total pressure distributions for the smaller span anhedral model at $\alpha = 8^{o}$.

Flow visualization

In the flow visualization photographs, the light rectangular patches are merely reflections from tape covering the model mounting screws. The thin light bands near the leading edges indicate where transition was fixed (5% c). In a few instances, natural transition can also be seen in regions where small portions of the trip strip have been blown away. The seepage of oil under the strip tends to weaken the adhesive bonding between strip and model surface. In the outboard portions of the wings, the dark patches bounded by light filaments, indicate regions where oil has been "washed" off the surface by vortex flow.

The flow over the wings is basically unseparated up to angles of attack of 12^{o}. One would not expect the spanwise center of lift to vary appreciably with angle of attack in the linear lift range. As a consequence, the rolling moment will vary linearly with lift.

Fig. 6 shows the upper-surface flow development for the planar configurations at an angle of attack of 12^{o}. For the smaller span baseline wing, Fig. 6 (a), the model-floor interference region occupies roughly 5% of wing area and the tip vortex region comprises roughly 5% of the wing area. The flow over the elliptical tip is relatively clean, Fig. 6 (b). This makes it difficult to quantify the proportion of oil washed off by the tip vortex. In the tip region, the trip strip has blown away and natural transition can be observed.

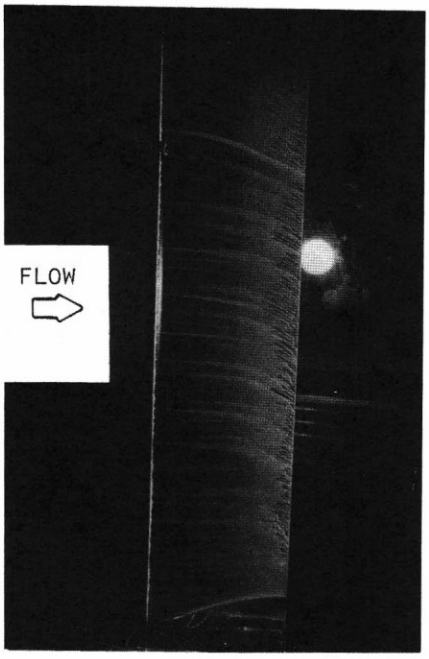

(a) Baseline.

Fig. 6 Upper surface flow visualization for the smaller span planar models at $\alpha = 12^{o}$.

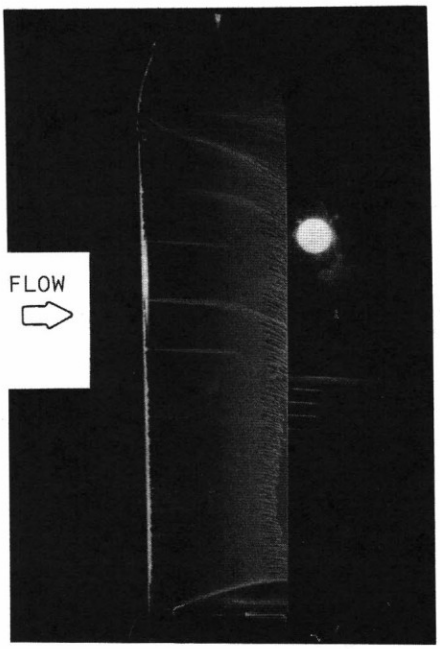

(b) Elliptical.

Fig. 6 Continued.

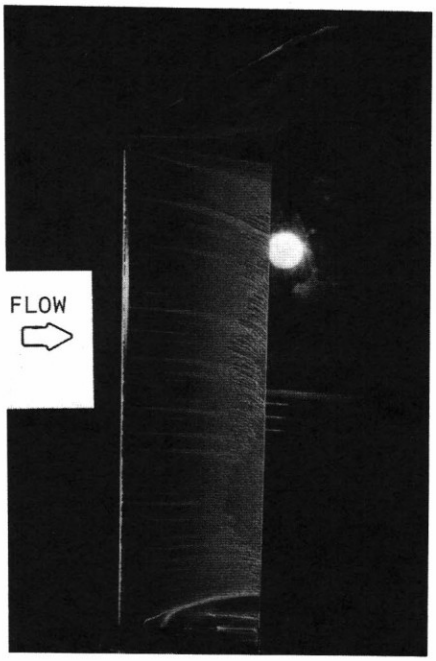

(c) Sheared.

Fig. 6 Concluded.

The swept and tapered outboard planform shows the strong vortex activity near the tip, Fig. 6 (c). The flow pattern suggests that there are three vortex systems in effect on the tip simultaneously; a separation induced leading edge vortex, a tip vortex and a secondary vortex (that sheds from the junction of the inboard rectangular planform with the outboard swept and tapered planform).

Fig. 7 shows the upper surface flow patterns for all the smaller span models at 18^{o}. There is basically large scale separation over wings and the mushroom cells are so large that a single saddle[26] point is difficult to pinpoint. The amount of flow separation (not including the floor interference and tip wash) is quantified in Table 7. This table also lists the distances between the eddy (mushroom cell) foci.

A vortex horn seems to emanate from the roughly the midpoint of the leading edge of the swept portion of the planar sheared wing. All three planar planforms have roughly the same amount of separated flow in this post-stall regime, Table 7. At this angle of attack, the nonplanar wings have larger proportions of separated flow than their planar counterparts.

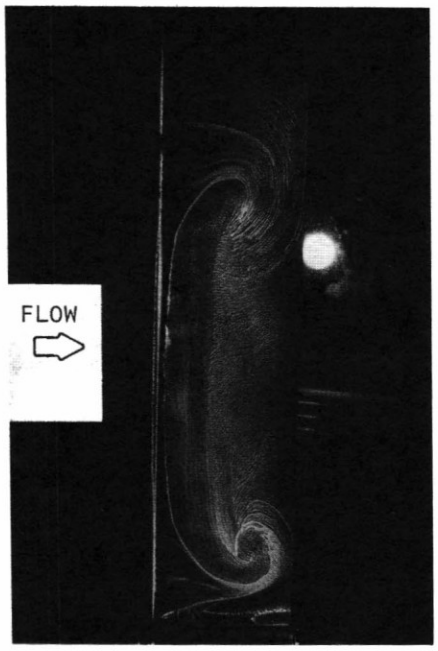

(a) Baseline.

Fig. 7 Upper surface flow visualization for the smaller span models at $\alpha = 18^{o}$.

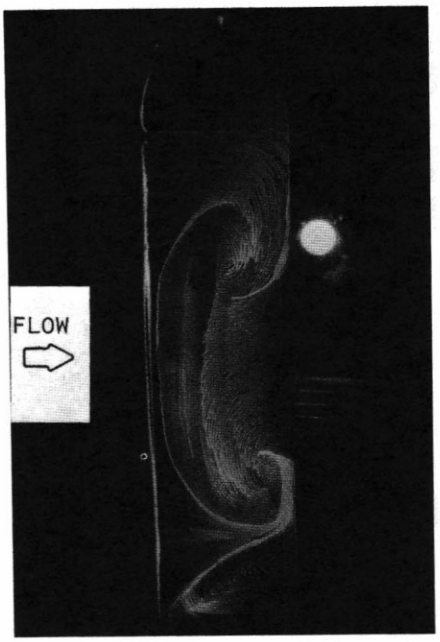

(b) Elliptical.

Fig. 7 Continued.

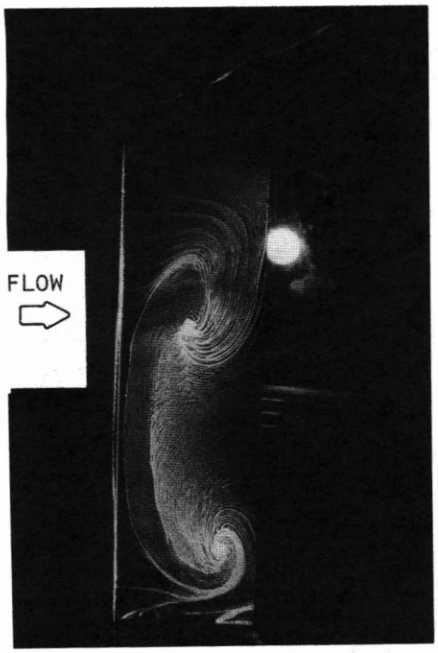

(c) Sheared.

Fig. 7 Continued.

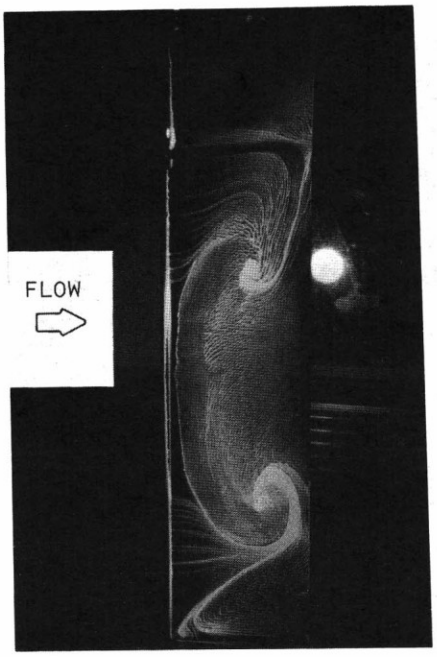

(d) Rising.

Fig. 7 Continued.

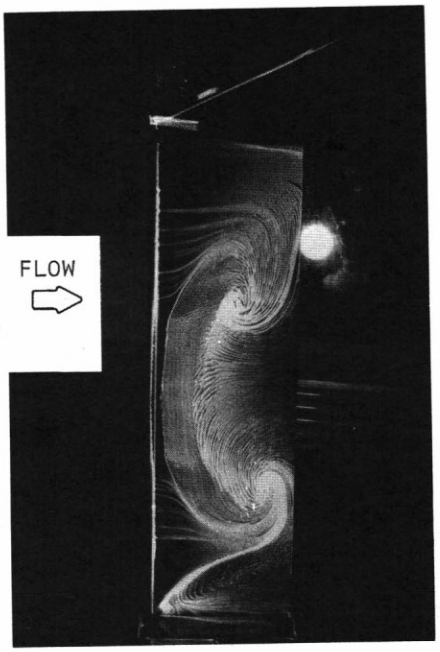

(f) Dihedral.

Fig. 7 Continued.

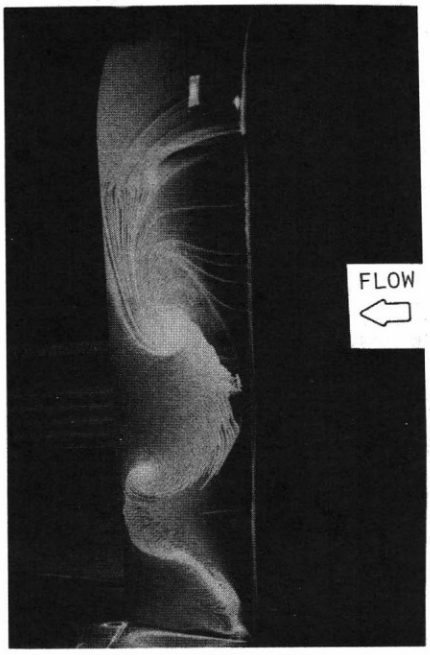

(e) Drooping.

Fig. 7 Continued

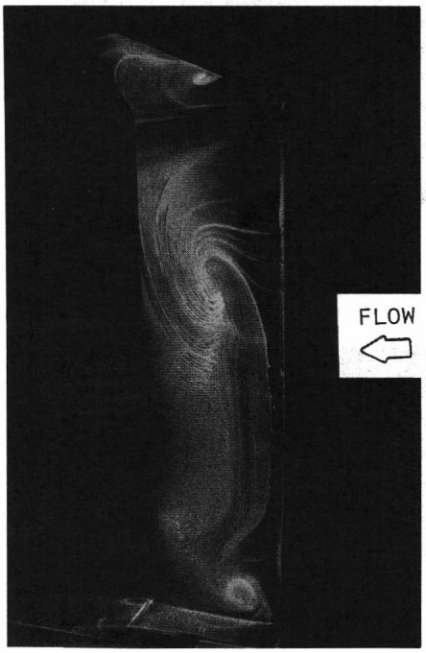

(g) Anhedral.

Fig. 7 Concluded.

Table 7 - Separated flow regions (as a percentage of total area) and cell foci distances for smaller span models at 18^{o}

Configuration	Separated flow (%)	Focus (x2/b)
Baseline	56	0.58
Elliptical	48	0.36
Sheared	51	0.39
Rising	75	0.38
Drooping	60	0.24
Dihedral	56	0.33
Anhedral	60	----

The longer span wings cannot support a single large mushroom cell. Instead, there are sub-cells. A representative structure is shown, in Fig. 8, for a larger span dihedral model at an angle of attack of 18^{o}. The lower sub-cell is of the same extent as the single mushroom cell on the smaller span model. Sixty percent of the upper surface of this dihedral model is separated.

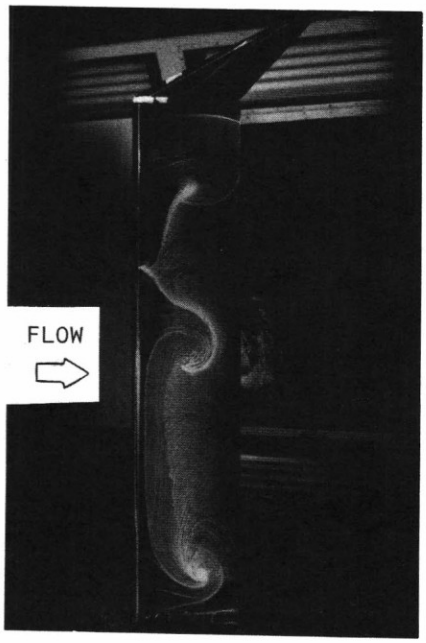

Fig. 8 Upper surface flow visualization for the larger span dihedral model at $\alpha = 18^{o}$.

IV. Conclusions and recommendations

For nonplanar planforms, span efficiency factors greater than one have been predicted by other researchers using lifting line theory and panel methods. This study supports this contention. The present experiments indicate that an experimentally derived span efficiency greater than one is possible for a non-planar wing. The induced drag benefits of wings with nonplanar outboard planforms are believed to accrue from the movement of vorticity away from the center of span line.

The effective span, as determined by the tip vortex, alone is not a sufficient yardstick for the induced performance of a non-planar wing. Rather, both the position of the vortex and its effect on the wing's downwash distribution is critical.

The possible disadvantages that could accrue when the lateral stability derivatives are calculated, particularly for the nonplanar wings, must be investigated. This analysis is beyond the scope of the present work.

References

[1]Naik, D. A. and Ostowari, C., "Experimental Investigation of Non-Planar Sheared Outboard Wing Planforms," AIAA 88-2549, AIAA 6th Applied Aerodynamics Conference, Williamsburg, Virginia, June 6th - 8th, 1988.

[2]Zimmer, H: "The Aerodynamic Optimization of Wings at Subsonic Speeds and the Influence of the Wingtip Design," NASA TM-88534, May 1987.

[3]Spillman, J. J., "The Use of Wing Tip Sails to Reduce Vortex Drag," Aeronautical Journal, September 1978, pp. 387-395.

[4]"Turbines Recover Power by Dissipating Induced Drag from Wingtip Vortices," Aviation Week and Space Technology, September 1, 1986, pp. 199.

[5] Hoerner, S.F., Fluid-Dynamic Drag, published by the author, Box 342, Brick Town, NJ 08273, 1965.

[6]Heyson, H. H., Riebe, G. D. and Fulton, C. L., "Theoretical Parametric Study of the Relative Advantages of Winglets and Wing-Tip Extensions," NASA-TP-1020, September 1977.

[7]Zimmer, H., "The Significance of Wing End Configuration in Airfoil Design for Civil Aviation Aircraft," NASA TM-75711, October 1979.

[8]Lundry, J. L., "A Numerical Solution for the Minimum Induced Drag, and the Corresponding Loading, of Nonplanar Wings," NASA CR-1218, November 1968.

[9]Gilkey, R. D., "Design and Wind Tunnel Tests of Winglets on a DC-10 Wing," NASA CR-3119, April 1979.

[10]Weihs, D. and Ashenberg, J., "Minimum Induced Drag of Wings with Curved Planform," AIAA Journal of Aircraft, Vol. 21, No. 1, January 1984, pp. 89-91.

[11]van Dam, C. P., "Induced-Drag Characteristics of Crescent-Moon-Shaped Wings," AIAA Journal of Aircraft, Vol. 24, No. 2, February 1987, 115-119.

[12]Maskew, B., "Prediction of Subsonic Aerodynamic Characteristics: A Case for Low-Order Panel Methods," AIAA Journal of Aircraft, Vol. 19, No. 2, February 1982, pp. 157-163.

[13]Maskew, B., "PROGRAM "VSAERO" - A Computer Program for Calculating the Non-Linear Aerodynamic Characteristics of Arbitrary Configurations," NASA CR-166476, December 1982.

[14]Cone, Jr., C.D., "The Theory of Induced Lift and Minimum Induced Drag of Nonplanar Lifting Systems," NASA TR R-139, 1962.

[15]Torenbeek, E., Synthesis of Subsonic Airplane Design, Student Edition, Delft University Press, Delft, The Netherlands, 1981, pp. 232-241.

[16]van Dam, C. P., "Analysis of Nonplanar Wing-Tip-Mounted Lifting Surfaces on Low-Speed Airplanes," NASA CR-3684, June 1983.

[17]van Dam, C. P., "Swept Wing-Tip Shapes for Low-Speed Airplanes," SAE Technical Paper 851770, October 1985.

[18]Narramore, J.C., Wentz, Jr., W.H., and Ostowari, C., "Evaluation of a Procedure for the Design of Low-Speed Airfoils: Analytical and Experimental Results for a 15% thick Symmetrical Section Airfoil with Control System," Wichita State University, Wichita, Kansas, AR 79-5, October 1979.

[19]Eppler, R., and Sommers, D.M., "A Computer Program for the Design and Analysis of Low Speed Airfoils," NASA TM 80210, August 1980.

[20]Rhode, R. V., "The Influence of Tip Shape on the Wing Load Distribution as Determined by Flight Tests," NACA R 500, 1934.

[21] Rae, Jr., W.H., and Pope, A., Low-Speed Wind Tunnel Testing, Second Edition, John Wiley & Sons, New York, 1984.

[22]Anderson, Jr., J. D., Introduction to Flight, 2nd. Edition, McGraw-Hill Book Company, New York, 1985, pp. 213-221.

[23]Francis, M. S. and Kennedy, D. A., "Formation of a Trailing Vortex," AIAA Journal of Aircraft, Vol. 16, No. 3, March 1979, pp.148-154.

[24]Reed, L., Mattingly, J. D. and Jonas, F. M., "The Seven-Hole Pressure Probe," USAFA-TN-84-9, USAF Academy, Colorado, 1984.

[25]Higuchi, H., Quadrell, J. C. and Farell, C., "Vortex Roll-up for an Elliptically-Loaded Wing at Moderately Low Reynolds Numbers," AIAA-86-0562, January 1986.

[26]Kuchemann, D., The Aerodynamic Design of Aircraft, Pergamon Press, Oxford, 1978.